Clinical Chemistry 59:11
000–000 (2013)

First Metabolic Profile of XLR-11, a Novel Synthetic Cannabinoid, Obtained by Using Human Hepatocytes and High-Resolution Mass Spectrometry

Ariane Wohlfarth,[1] Shaokun Pang,[2] Mingshe Zhu,[3] Adarsh S. Gandhi,[1] Karl B. Scheidweiler,[1] Hua-fen Liu,[2] and Marilyn A. Huestis[1*]

BACKGROUND: Since the mid-2000s synthetic cannabinoids have been abused as recreational drugs, prompting scheduling of these substances in many countries. To circumvent legislation, manufacturers constantly market new compounds; ((1-[5′fluoropentyl]indol-3-yl)-(2,2,3,3-tetramethylcyclopropyl)methanone (XLR-11), the fluorinated UR-144 analog, is one of the most recent and widely abused drugs, and its use is now linked with acute kidney injury. Our goal was to investigate XLR-11 metabolism for identification of major urinary targets in analytical methods and to clarify the origin of metabolites when one or more parent synthetic cannabinoids can be the source.

METHODS: We incubated 10 μmol/L XLR-11 with pooled human hepatocytes and sampled after 1 and 3 h. Samples were analyzed by high-resolution mass spectrometry with a TOF scan followed by information-dependent acquisition triggered product ion scans with dynamic background subtraction and mass defect filters. Scans were thoroughly data mined with different data processing algorithms (Metabolite Pilot 1.5).

RESULTS: XLR-11 underwent phase I and II metabolism, producing more than 25 metabolites resulting from hydroxylation, carboxylation, hemiketal and hemiacetal formation, internal dehydration, and further glucuronidation of some oxidative metabolites. No sulfate or glutathione conjugation was observed. XLR-11 also was defluorinated, forming UR-144 metabolites. On the basis of mass spectrometry peak areas, we determined that the major metabolites were 2′-carboxy-XLR-11, UR-144 pentanoic acid, 5-hydroxy-UR-144, hydroxy-XLR-11 glucuronides, and 2′-carboxy-UR-144 pentanoic acid. Minor metabolites were combinations of the biotransformations mentioned above, often glucuronidated.

CONCLUSIONS: These are the first data defining major urinary targets of XLR-11 metabolism that could document XLR-11 intake in forensic and clinical investigations.

Synthetic cannabinoids are cannabinoid 1 (CB_1)[4] and/or CB_2 receptor ligands originally developed as pharmacological tools for investigating the endocannabinoid system or as potential pharmacotherapies. Hundreds of compounds were synthesized in academia and pharmaceutical companies, and their binding affinities and structure-activity relationships were investigated *(1–3)*. Since the mid-2000s these designer drugs have been abused as recreational drugs *(4–5)*, leading to numerous intoxications as demonstrated by the high number of poison control calls *(6)* and emergency department visits over the last few years *(7)*, and also demonstrated by surveys among adolescents that showed high prevalence *(8–9)*. Identifying which substances are currently on the market is a substantial challenge for forensic and clinical laboratories, as well as developing analytical methods for new designer drugs, which requires knowledge of the drugs' metabolism. Synthetic cannabinoids are almost exclusively excreted as metabolites in urine *(10–16)*, the most common screening matrix in clinical, workplace, military, and sport doping drug testing. Therefore, knowledge of urinary metabolites is required for developing effective urine testing methods, but no data on the human metabolism of new compounds are available. Be-

[1] Chemistry and Drug Metabolism, Intramural Research Program, National Institute on Drug Abuse, National Institutes of Health, Baltimore, MD; [2] AB SCIEX, Foster City, CA; [3] Department of Biotransformation, Bristol-Myers Squibb Research and Development, Princeton, NJ.
* Address correspondence to this author at: Chemistry and Drug Metabolism, IRP, National Institute on Drug Abuse, National Institutes of Health; Biomedical Research Center; 251 Bayview Blvd. Suite 200 Rm. 05A-721, Baltimore, MD 21224. Fax 443-740-2823; e-mail mhuestis@intra.nida.nih.gov.

Received May 17, 2013; accepted August 20, 2013.
Previously published online at DOI: 10.1373/clinchem.2013.209965

[4] Nonstandard abbreviations: CB_1, cannabinoid 1; XLR-11, ((1-[5′fluoropentyl]indol-3-yl)-(2,2,3,3-tetramethylcyclopropyl)methanone; TMCP, 2,2,3,3-tetramethylcyclopropyl; K_i, receptor-binding affinity; MS, mass spectrometry; LC, liquid chromatography; IDA, information-dependent acquisition; MS/MS, tandem MS; RT, retention time.

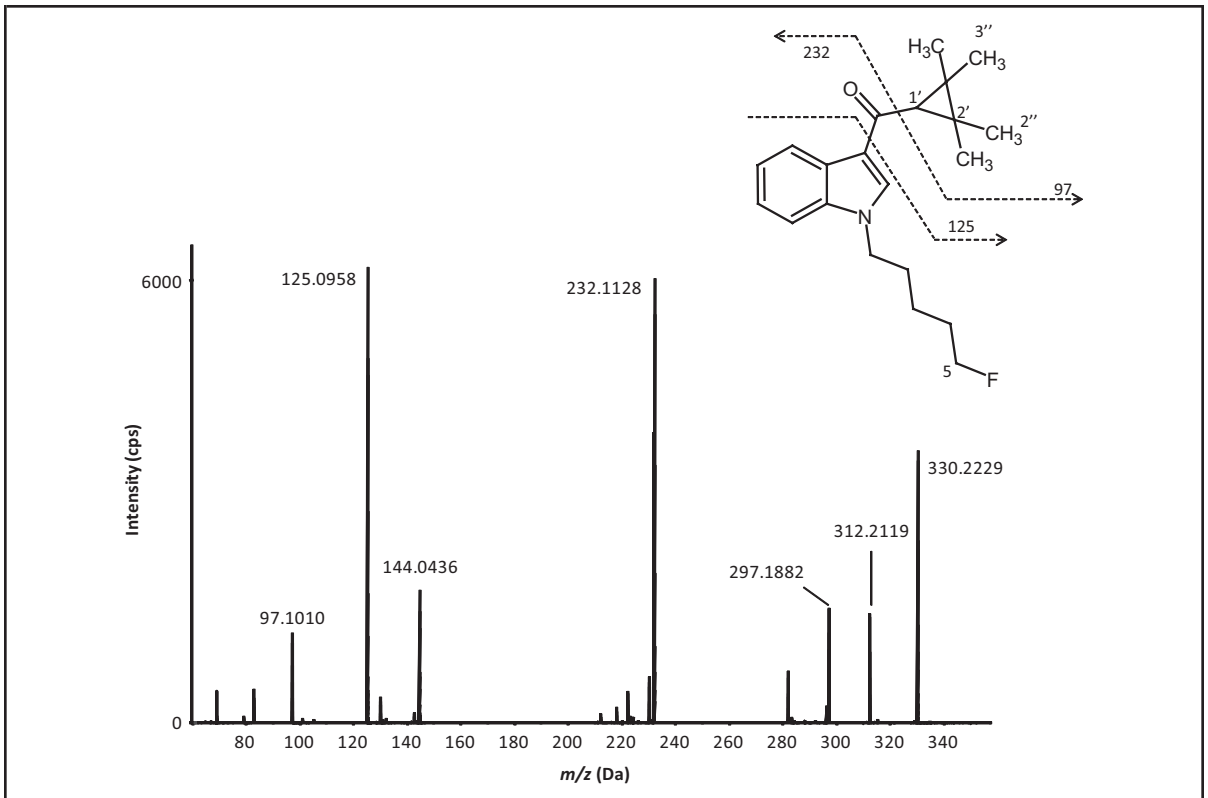

Fig. 1. MS/MS spectrum and structure of XLR-11 with assigned fragmentation pattern, and labeling of metabolic sites.

cause approval for controlled administration studies in humans cannot be obtained owing to a lack of toxicological data, other strategies are necessary to determine major metabolic targets.

As rapidly as synthetic cannabinoids were scheduled, new compounds emerged. The most popular naphthoylindoles (e.g., JWH-018, AM2201), as well as phenacetylindoles, benzoylindoles, and whole structural classes were scheduled in most European countries, the US, Japan, Russia, Australia, and New Zealand. Consequently, clandestine laboratories synthesized similar nonregulated compounds. One of the newest compounds is ((1-[5′fluoropentyl]indol-3-yl)-(2,2,3,3-tetramethylcyclopropyl)methanone (XLR-11) (Fig. 1), which replaced former popular substances like AM2201 and JWH-018. XLR-11 is not currently covered by most of the regulations owing to its unusual structural element, the 2,2,3,3-tetramethylcyclopropyl (TMCP) ring. In May 2013, the US Drug Enforcement Administration temporarily placed XLR-11 into Schedule I of the Controlled Substance Act *(17)*. XLR-11 was detected in late 2011 in Russia *(18)* and also was reported in Japan *(19)*, Europe *(20)* and the US *(21)*. According to several reports *(17, 21)*, XLR-11 prevalence in the US has increased significantly since the summer of 2012 and remained increased in the beginning of 2013.

TMCP cannabinoids were developed by Abbott Laboratories; synthesis and cannabinoid receptor affinities for 70 compounds were published in 2010 *(1)*. Investigators reported that the TMCP group generally has high CB_2 affinity not related to preferred subjective drug effects. Although XLR-11, which has a 5-fluoropentyl side chain at the indole nitrogen, is not mentioned in this publication, the assessment of receptor affinities for 2 closely related compounds, one with a nonfluorinated pentyl side chain and the other with a 5,5,5-trifluoropentyl side chain, was reported. The first compound, also known as UR-144, has high CB_2 but low CB_1 receptor-binding affinity (K_i) (K_i CB_1, 150 nmol/L; *Ki* CB_2, 1.8 nmol/L), whereas the second compound showed high CB_1 receptor affinity (*Ki* CB_1, 15 nmol/L; *Ki* CB_2, 0.09 nmol/L) *(1)*.

The purpose of this study was to investigate human XLR-11 metabolism by analyzing samples collected after drug incubation with human hepatocytes with high-resolution mass spectrometry (MS) and software-assisted data mining. This approach creates realistic metabolic profiles because enzyme activities in human hepatocytes produce metabolite concentra-

tions in ratios similar to those found in vivo. Compared to other approaches, e.g., incubation with human liver microsomes or controlled drug administration to rats, human hepatocytes provide the most authentic spectrum of metabolites. Microsomes do not produce phase II metabolites. XLR-11 was selected for this research because of its current high prevalence, the lack of any knowledge on its metabolism in humans, and the serious acute kidney injuries described in adolescents that were associated with XLR-11 in several cases *(22–23)*. Although XLR-11 has not been proven as the causative agent, the parent compound was detected in the implicated product or toxicological results strongly suggested XLR-11 (detection of parent compound in serum or UR-144 pentanoic acid in urine).

Materials and Methods

CHEMICALS AND REAGENTS

XLR-11 was obtained from Cayman Chemicals, formic acid for LC-MS from Fisher Scientific, and LC-MS–grade acetonitrile from Sigma Aldrich. Water was purified in house with an ELGA Purelab Ultra Analytic purifier (Siemens Water Technologies).

INCUBATION WITH HUMAN LIVER HEPATOCYTES

XLR-11 was incubated at a final substrate concentration of 10 μmol/L with pooled cryopreserved human hepatocytes from 3 donors (Celsis InVitro Technologies) under shaking in an incubator at 37 °C. A 1-mL suspension containing 1.3 million hepatocytes/mL with viability of >80% was used. Samples were collected after 0, 1, and 3 h of incubation, mixed with an equal volume of, and stored at −80 °C until analysis. A positive control sample with diclofenac was incubated with XLR-11 and was analyzed for expected metabolites, 4′-hydroxydiclofenac and diclofenac acyl glucuronide, to ensure metabolite formation under the given experimental conditions.

SAMPLE PREPARATION

Samples were clarified via centrifugation at 15 000*g*, 4 °C for 5 min and diluted 1:4 with mobile phase before 10 μL injection. The blank mobile phase, a neat 50 μg/L XLR-11 standard in mobile phases A and B (50/50, vol/vol), and the 0 h-sample were analyzed as controls.

INSTRUMENTATION

Samples were chromatographed on a Shimadzu Prominence HPLC system that consisted of 2 LC-20AD XR pumps, a DGU-20A5R degasser, a SIL-20AC XR autosampler, and a CTO-20 AC column oven. MS data were acquired on an AB SCIEX Triple TOF 5600 instrument controlled with AB SCIEX Analyst TF (version 1.6) software. Metabolite Pilot (version 1.5) was used for data mining and structure elucidation. A Shimadzu LC-10AD pump and a 10-port W-type diverter valve (VICI; Valco Instruments) delivered a make-up solution into the ion source in the time periods when the liquid chromatography (LC) flow was diverted to waste. This is recommended for keeping the MS instrument calibration stable.

CHROMATOGRAPHIC CONDITIONS

Gradient elution was performed on a Kinetex C18 XB column (100 mm × 2.1 mm, 2.6 μm) fitted with a KrudKatcher Ultra HPLC in-Line cartridge (0.5 μm × 0.1 mm ID, Phenomenex) at 40°C with 0.1% formic acid in water (mobile phase A) and 0.1% formic acid in acetonitrile (mobile phase B) at a flow rate of 0.3 mL/min. Gradient conditions were: 10% B until 0.3 min, increased to 20% B at 0.5 min, to 80% B at 20.0 min, to 95% B at 20.1 min and held for 1.8 min before column reequilibration at 10% B for 3.0 min. Total run time was 25.0 min. The autosampler temperature was 4°C.

MASS SPECTROMETRY

The MS method consisted of a TOF MS survey scan and an information-dependent acquisition (IDA)-triggered TOF tandem MS (MS/MS) scan with positive electrospray ionization. Source parameters were: source temperature 500 °C, ionspray voltage 5500 V, ion source gas 1 50 *ψ*, ion source gas 2 50 *ψ*, curtain gas 30 *ψ*. The TOF scan range was *m/z* 100–950 Da, with an accumulation time of 0.1 s. The declustering potential was optimized and set to 140 V; the collision energy was 10 eV.

Data were acquired by IDA experiments with dynamic background subtraction with the following specifications: exclusion of isotopes within 3 Da, no exclusion of former target ions, and mass tolerance 50 mDa. Each sample was analyzed with and without mass defect filtering. Mass defect filtering was set with a mass tolerance of 40 mDa for metabolites similar to the parent drug or with major modifications, e.g., dealkylation or glucuronidation, which would markedly change the mass defect (Table 1). A maximum of 4 candidate ions were selected for subsequent product ion scans based on signal intensity. Product ion scans were acquired from 60–950 Da with an accumulation time of 0.075 s per scan. The declustering potential was 140 V. The collision energy was optimized and set to 40 eV with a spread of ±10 eV. External mass calibration was performed automatically every fifth injection via infusion through the Calibrant Delivery System.

DATA PROCESSING AND EVALUATION OF CANDIDATES

Data processing was performed with MetabolitePilot software (AB SCIEX). A set of biotransformations for processing the data and assigning appropriate metabolites was created on the basis of the structure of XLR-11. Peaks were considered for metabolite search and MS/MS fragment interpretation if they corresponded

Table 1. Mass defect filters for XLR-11 utilized during data acquisition and data mining.

Biotransformation	Formula	Molecular weight, Da	Width, Da	Mass defect, mDa
Parent	$C_{21}H_{28}NOF$	329.2155	100	215.4930
Glucuronidation	$C_{27}H_{36}NO_7F$	505.2476	100	247.5812
Glutathione conjugation	$C_{13}H_{45}N_4O_7FS$	636.2993	100	299.3004
Sulfation	$C_{21}H_{28}NO_4FS$	409.1723	100	172.3087
C5-dealkylation	$C_{16}H_{19}NO$	241.1467	100	146.6644
Defluorination	$C_{21}H_{29}NO$	311.2249	100	224.9148
C5-dealkylation and glucuronidation	$C_{22}H_{27}NO_7$	417.1788	100	178.7526
Defluorination and glucuronidation	$C_{21}H_{37}NO_7$	487.2570	100	257.0030

to a predicted mass, were within the range of calculated mass defect filters, or showed at least 2 characteristic product ions/neutral losses. The minimum peak width was 2.5 s, minimum peak intensity 1500 cps, MS *m/z* tolerance 40 ppm, and minimum MS peak intensity 400 cps. The maximum number of unexpected metabolites was restricted to 10. The identified peaks were confirmed as metabolites based on mass accuracy as well as plausible retention time and fragmentation. Major metabolites were determined on the basis of MS peak area ranks, which were assigned within the 1-h and 3-h samples, respectively.

Results

XLR-11 was metabolized by phase I and II enzymes in human hepatocytes; more than 25 XLR-11metabolites were produced by hydroxylation, carboxylation, hemiketal and hemiacetal formation, internal dehydration, and further glucuronidation of some oxidative metabolites. Mass shifts of the proposed structures compared to calculated exact masses were <2.7 ppm for all metabolites. Retention times were between 5.75 and 13.85 min, with XLR-11 eluting at 17.3 min (Fig. 2A), which provided sufficient time for potential later-eluting metabolites like N-oxides in the 20-min gradient. Notably, XLR-11 also underwent oxidative defluorination resulting in UR-144 metabolites. Table 2 lists all metabolites with retention times, exact masses, assigned biotransformation(s), major fragments, and rank based on MS peak area in the 1-h and 3-h samples. Metabolites resulted from hydroxylation (M6, M7, M8, M14, M17, M18, M20, M21) with subsequent ring closure (M23, M30), carboxylation (M11, M13, M14, M18, M27), and oxidative defluorination (M10, M12, M15, M16, M19, M23, M24, M28, M29). Many metabolites underwent further glucuronidation (M1–9, M11, M13, M17, M20–22, M25, M26). Accurate mass measurements and retention times suggested less common metabolic reactions, e.g., hemiacetal formation for M7, M9, and M22, hemiketal formation for M24, and internal dehydration for M23 and M30. No sulfate or glutathione conjugation was observed.

Main sites of metabolic modifications were (*a*) the terminal position of the pentyl side chain, (*b*) the TMCP ring, and (*c*) the α-carbon atom next to the carbonyl function. Based on MS peak areas and ranking in the 1-h and 3-h samples, the main XLR-11 metabolites were 2′-carboxy-XLR-11 (M27), UR-144 pentanoic acid (M28), 5-hydroxy-UR-144 (M29), 2′-carboxy-UR-144 pentanoic acid (M15), and the 3 hydroxy-XLR-11 glucuronides (M21, M18, M20).

Discussion

High-resolution MS acquiring full-scan MS and MS/MS data provides a powerful tool for metabolite identification. The formula of the intact molecule is accurately determined, and accurate mass measurements aid in assigning correct fragment structures. Structure elucidation is easier and faster than with conventional MS requiring multiple injections for precursor ion, neutral loss, and product ion scans.

Some limitations to these first predictions of XLR-11 metabolism should be considered. First, human hepatocytes cannot fully substitute for the complex interactions and processes occurring during metabolism and elimination from the human body. Although human hepatocytes offer the most realistic conditions to determine the metabolic profile of a substance compared with other biological systems, these results predict which metabolites will most likely be found in humans. Second, the cyclopropyl ring is under strain and has been shown to be unstable under certain conditions. Shevyrin et al. *(18)* and Kavanagh et al. *(24)* proposed ring opening during 2,2,3,3-TMCP cannabinoid stability studies. The cyclopropyl ring can be cleaved when heated, forming isomers carrying a pent-4-en-1-one chain. The extent to which this isomerization occurs is unclear, but it should be con-

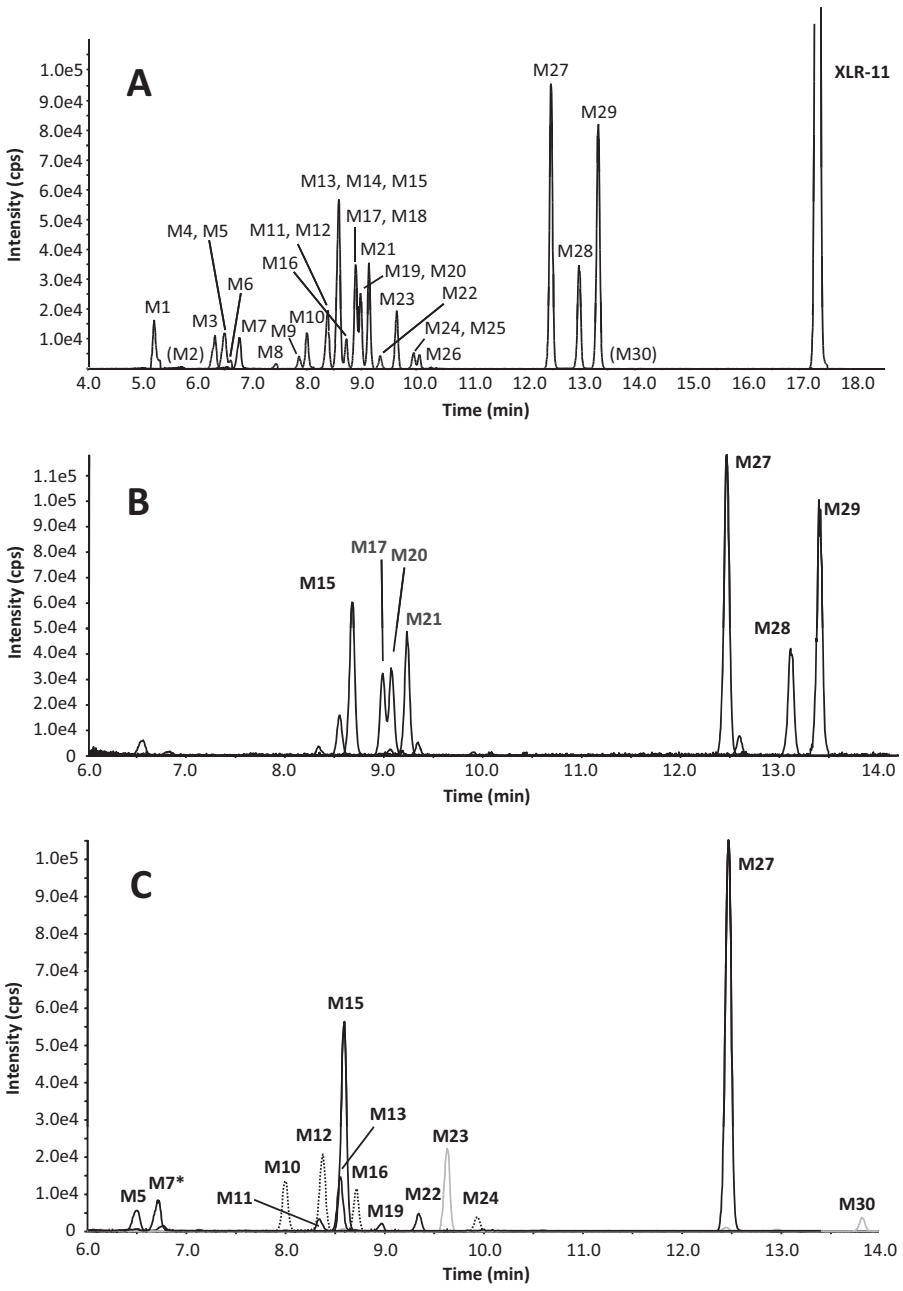

Fig. 2. Extracted ion chromatogram from 4–18 min showing all metabolites found in the 3h sample, labeled with metabolite numbers from Table 2.

M2 and M30 were detected in the 1 h sample only and are given in parentheses (A). Extracted ion chromatogram from 6–14 min of the 3 h sample showing the seven major metabolites (B). Extracted ion chromatogram from 6–14 min of the 3 h sample for particular metabolites at *m/z* 358 (dotted line), *m/z* 360 (bold black line), *m/z* 372 (thin black line), *m/z* 342 (M30, grey line) and *m/z* 356 (M23, grey line) that are discussed in detail in the text (C).

* The peak of M7 belongs to *m/z* 548, the corresponding glucuronide of *m/z* 372.

Table 2. List with all metabolites sorted by retention time with molecular weight, major fragments, a rank of the corresponding peak area in the 1-h and the 3-h -sample, and a description of the biotransformation.

Metabolite ID	RT, min	Name	Description	*m/z* [M-H]+	Major fragments
M0	17.33	Parent		330.2235	97, 125, 144, 232, 297
M1	5.21	Not assigned (oxidative defluorination to carboxylic acid confirmed)	−F +2O −3H	340.1910	144, 244
M2	5.75	Oxidative defluorination to carboxylic acid + glucuronidation	−F +2O −H +$C_6H_8O_6$	342.2062[a]	144, 244
M3	6.33	Oxidative defluorination + oxidation + glucuronidation	−F +2O +H +$C_6H_8O_6$	520.2535	144, 230, 326, 344
M4	6.49	Oxidative defluorination + oxidation + glucuronidation	−F +2O +H +$C_6H_8O_6$	520.2534	144, 230, 326, 344
M5	6.51	Oxidative defluorination to carboxylic acid + carboxylation + glucuronidation	−F −3H +4O +$C_6H_8O_6$	372.1807[a]	144, 244, 344
M6	6.62	Di-oxidation + glucuronidation	+2O +$C_6H_8O_6$	538.2434	144, 248, 344, 362
M7	6.76	Oxidative defluorination to carboxylic acid + oxidation + aldehyde formation followed by hemiacetal formation and glucuronidation	−F −3H +4O + $C_6H_8O_6$	548.2100	144, 218, 244, 354, 372
M8	7.44	Tri-oxidation + glucuronidation	+3O +$C_6H_8O_6$	554.2389	232, 360, 378
M9	7.86	Oxidative defluorination + oxidation + glucuronidation	−F +2O +H +$C_6H_8O_6$	520.2534	125, 246, 344
M10	8.00	Oxidative defluorination to carboxylic acid + oxidation	−F −H +3O	358.2016	144, 244
M11	8.33	Carboxylation + glucuronidation (diastereomer 1)	+2O −2H + $C_6H_8O_6$	360.1980[a]	206, 232, 298, 342
M12	8.38	Oxidative defluorination to carboxylic acid + oxidation	−F −H +3O	358.2016	144, 244
M13	8.54	Carboxylation + glucuronidation (diastereomer 2)	+2O −2H + $C_6H_8O_6$	536.2294	206, 232, 342
M14	8.56	Carboxylation + oxidation	+3O −2H	376.1919	144, 204, 248, 314, 358
M15	8.58	Oxidative defluorination to carboxylic acid + carboxylation	−F −3H +4O	372.1811	144, 244, 310, 354
M16	8.72	Oxidative defluorination + carboxylation	−F −H +3O	358.2016	144, 204, 230, 340
M17	8.89	Oxidation + glucuronidation	+O + $C_6H_8O_6$	522.2491	144, 232, 328, 346
M18	8.89	Carboxylation + oxidation		376.1923	248, 268, 358
M19	8.96	Oxidative defluorination to carboxylic acid + oxidation + aldehyde formation followed by hemiacetal formation	−F −3H +4O	372.1812	144, 244, 354
M20	8.98	Oxidation + glucuronidation	+O +$C_6H_8O_6$	522.2494	144, 232, 328, 346
M21	9.13	Oxidation + glucuronidation	+O +$C_6H_8O_6$	522.2497	144, 232, 328, 346
M22	9.33	Oxidation + aldehyde formation followed by hemiacetal formation + glucuronidation	+2O −2H +$C_6H_8O_6$	536.2294	144, 155, 232, 298, 342
M23	9.64	Oxidative defluorination to carboxylic acid + Di-oxidation followed by internal dehydration	−F +3O −3H	356.1858	144, 244
M24	9.94	Oxidative defluorination to carboxylic acid + oxidation + hemiketal formation	−F −H +3O	358.2012	144, 200, 244, 274

Continued on page XX

Table 2. List with all metabolites sorted by retention time with molecular weight, major fragments, a rank of the corresponding peak area in the 1-h and the 3-h -sample, and a description of the biotransformation.
(Continued from page XX)

Metabolite ID	RT, min	Name	Description	*m/z* [M-H]+	Major fragments
M25	9.97	Oxidative defluorination to carboxylic acid + glucuronidation	−F −H +2O +$C_6H_8O_6$	518.238	125, 244, 342
M26	10.06	Oxidative defluorination + glucuronidation	−F +H +O +$C_6H_8O_6$	504.2595	125, 230, 328
M27	12.47	Carboxylation	+2O −2H	360.1976	206, 232, 342
M28	12.98	Oxidative defluorination to carboxylic acid	−F −H +2O	342.2073	125, 144, 244, 324
M29	13.33	Oxidative defluorination	−F +O +H	328.2279	97, 125, 144, 230
M30	13.85	Di-oxidation followed by internal dehydration	+O −2H	344.2019	144, 232

[a] Potential in-source-fragmentation of the glucuronidated metabolite because only the mass of the aglycone was found.

sidered since synthetic cannabinoids are primarily consumed by smoking.

XLR-11

Fig. 1 shows the product ion spectrum of XLR-11 [M0, *m/z* 330.2229, retention time (RT) 17.33 min]. We related 4 characteristic fragments to a substructure. The 2 most intense fragments are *m/z* 125, which indicates an intact TMCP ring with the vicinal carbonyl group, and *m/z* 232, which is the fluoropentyl indole moiety with the carbonyl group attached. Removal of the TMCP ring produces a minor fragment with *m/z* 97, whereas fragment *m/z* 144 is the dealkylated carbonyl indole moiety. The other product ions could not be assigned definitively. For structure elucidation of metabolites, mass shifts of product ions between the metabolite and the parent compound will indicate where structure modifications did or did not occur.

MAJOR METABOLITES

Major metabolites were determined by ranking MS peak areas at 1 h and 3 h and combining the results. Fig. 2B shows the extracted ion chromatograms for the 7 most abundant metabolites; Fig. 3 depicts their proposed structures and product ion spectra.

2′-Carboxy-XLR-11 (M27, *m/z* 360.1976, RT 12.47 min) is the most intense metabolite after 1 h and 3 h of incubation and is therefore the most important XLR-11 metabolite. To date, M27 is specific for identifying XLR-11 consumption. It shows characteristic fragments at *m/z* 144 and 232, suggesting an unchanged indole moiety and fluoropentyl chain. Indicated by *m/z* 155 and the absence of *m/z* 97 and *m/z* 125 fragment ions, the carboxylation occurs at 1 of the 4 methyl groups, which are stereoisomerically identical. A loss of 46 Da is another indicator for a carboxyl group producing an *m/z* 314 fragment.

UR-144 pentanoic acid (M28, *m/z* 342.2073, RT 12.98 min) is derived from XLR-11 after oxidative defluorination—a biotransformation that is already known to occur for other fluorinated synthetic cannabinoids like AM2201 (*(16)*). This metabolite displays characteristic product ions at *m/z* 97 and *m/z* 125, which are both related to an unaltered TMCP ring, and at *m/z* 144, an unchanged indole moiety. Fragment *m/z* 244 indicates that oxidative defluorination at the terminal position of the pentyl side chain occurred, followed by further oxidation. Notably, 5-carboxy-UR-144 is already commercially available. However, it is impossible to unambiguously distinguish between UR-144 and XLR-11 consumption by considering this metabolite only.

5-Hydroxy-UR-144 (M29, *m/z* 328.2279, RT 13.33 min) is the metabolic precursor of UR-144 pentanoic acid. Characteristic product ions were *m/z* 97, *m/z* 125, and *m/z* 144, suggesting that no modifications take place at the TMCP ring and the indole moiety. Fragment *m/z* 230 indicates defluorination and hydroxylation at the pentyl side chain. This metabolite also is commercially available to detect XLR-11 intake.

It is consistent that another major XLR-11 metabolite is generated by a combination of the biotransformations that led to the first 2 metabolites. The MS/MS spectrum of 2′-carboxy-UR-144 pentanoic acid (M15, *m/z* 372.1811, RT 8.58 min) shows fragments at *m/z* 218 and *m/z* 244, suggesting a carboxyl function at the end of the pentyl chain, with no modification at the indole moiety (*m/z* 144). We conclude that the second carboxylation will be located at the TMCP ring since there were no fragments at *m/z* 97 or *m/z* 125. The dominant fragment at *m/z* 354 is generated by a loss of

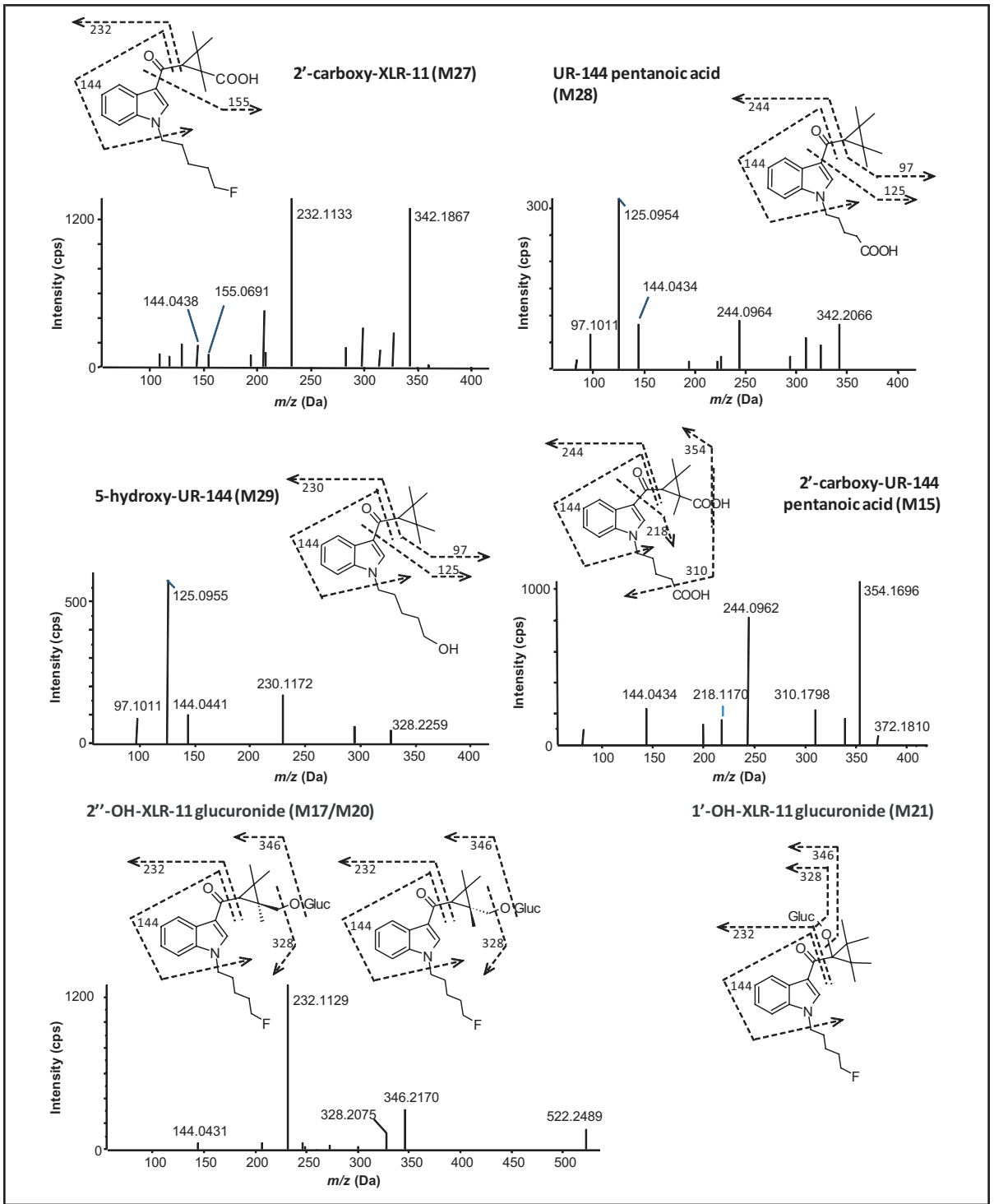

Fig. 3. Product ion spectra, structures and fragmentation of the seven major metabolites of XLR-11, chromatogram of the 3 h sample.

The chromatogram of M18 is representative for the other two hydroxy-XLR-11 glucuronides as well, which showed the same characteristic fragments.

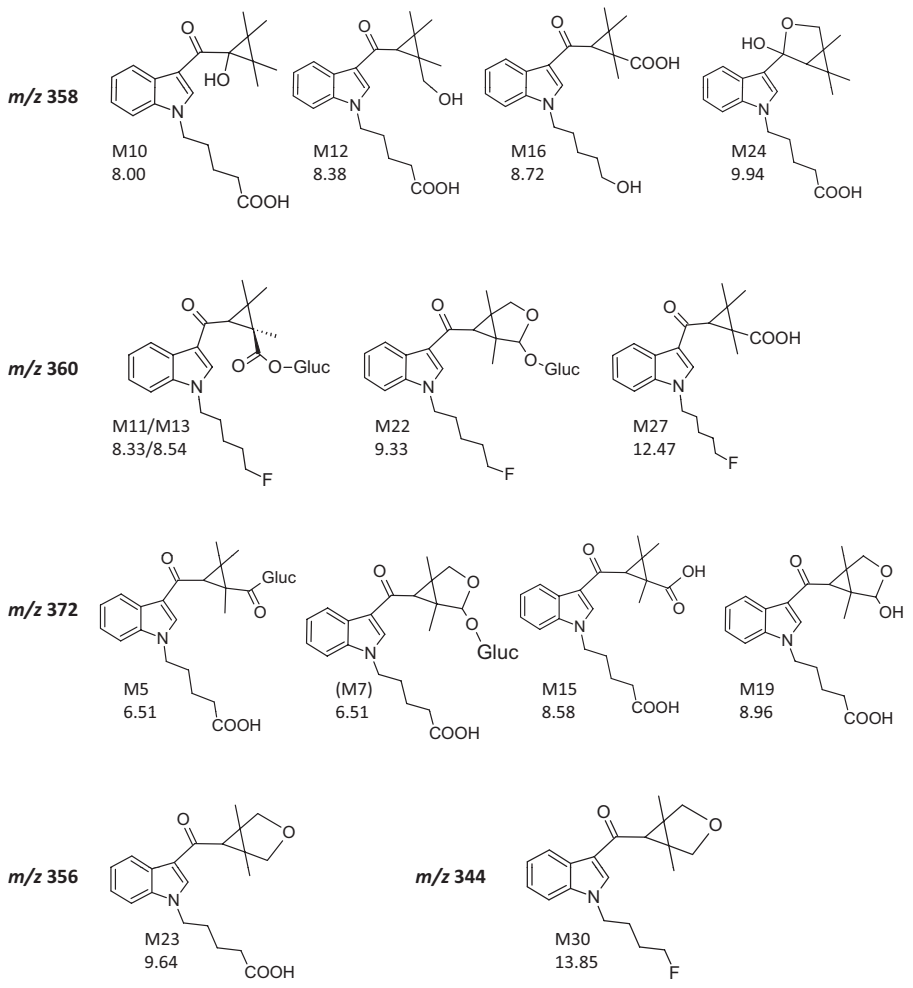

Fig. 4. Proposed structures for the metabolites with *m/z* 358, *m/z* 360, *m/z* 372, *m/z* 344 and *m/z* 356 that are discussed in detail in the text.

M12 and M14 are the two diastereomers of 2″-hydroxy-XLR-11 glucuronide. The conjugated metabolite M8 was detected at *m/z* 548 but is shown for explanatory reasons in the group of *m/z* 372.

water from the parent; subsequent decarboxylation leads to *m/z* 310.

Three hydroxy-XLR-11 glucuronides were found (M17, *m/z* 522.2491, RT 8.89 min; M20, *m/z* 522.2494, RT 8.98 min; and M21, *m/z* 522.2497, RT 9.13 min) (depicted in black in Fig. 2B), all of them showing fragments at *m/z* 144 and *m/z* 232, which are related to an unchanged indole moiety and fluorinated pentyl side chain. Consequently, the oxidation occurs at the remaining part of the molecule, raising the question why 3 peaks were observed when there are only 2 possible sites for the oxidation to take place. Although a hydroxy group at different methyl groups of the TMCP ring does not lead to sterically different molecules, the introduction of a second chiral center by glucuronidation does. Therefore, we assume that the 2 closely eluting substances (M17 and M20) are diastereomers of 2′-hydroxy-XLR-11 glucuronide, whereas the third compound eluting at 9.14 min (M21) is generated by oxidation at the 1′ position, followed by glucuronidation. Oxidation at the exposed methyl group is more likely to occur than at the α-carbon atom of a carbonyl function, which explains the peak intensities.

STRUCTURE ASSIGNMENTS FOR PARTICULAR METABOLITES (*m/z* 358, *m/z* 360, *m/z* 372, *m/z* 344, AND *m/z* 356)

Structure assignments that are particularly interesting are discussed in detail. Fig. 2C shows the extracted ion chromatograms; Fig. 4 presents the proposed structures. Four metabolites with a molecular ion at *m/z*

358—depicted in dotted line in Fig. 2C—were found at both time points (M10, *m/z* 358.2016, RT 8.00 min; M12, 358.2016, RT 8.38 min; M16, *m/z* 358.2016, RT 8.72 min; and M24, *m/z* 358.2012, RT 9.94 min), with a mass shift suggesting hydroxylation and carboxylation. Three metabolites—M10, M12 and M24—show fragments at *m/z* 144 and *m/z* 244 in their MS/MS spectra, which indicate oxidative defluorination to carboxylic acid at the pentyl side chain, leaving hydroxylation for the remaining part of the molecule. The MS/MS spectrum of the fourth metabolite, M16, gives a characteristic fragment at *m/z* 230, which occurs only for this compound and could be related to oxidative defluorination to form a 5-hydroxypentyl chain. The lack of *m/z* 97 and *m/z* 125 indicates carboxylation at the TMCP ring, most probably at an exposed methyl group. With similar product ion spectra and close retention times, M10 and M12 appear to be related, whereas M24 showed different fragments (*m/z* 200) and eluted later. We suggest that M10 is hydroxylated at the α-carbon atom while M12 is hydroxylated at a methyl group of the TMCP ring. This is in agreement with calculated logP (octanol–water partition coefficient) values (2.90 vs 2.96) *(25)* and peak intensities. We propose that M24 is a minor metabolite that is generated by hemiketal formation between the carbonyl group and the hydroxyl group.

In total 3 metabolites were observed with a molecular ion at *m/z* 372 (depicted in a thin black line in Fig. 2C). Whereas M5 (*m/z* 372.1807, RT 6.51 min) and M15 (*m/z* 372.1811, RT 8.58 min) were detected at both time points, M19 is a minor metabolite showing only a small signal in the 3-h sample (*m/z* 372.1812, RT 8.96). As already mentioned, M15 is one of the major metabolites, 2′-carboxy-UR-144 pentanoic acid. Based on its retention time, we conclude that M5 is the acyl glucuronide of this metabolite. Acyl glucuronides are known to be unstable; they can be cleaved during storage and insource fragmented in the mass spectrometer. Therefore, it is likely that the glucuronide underwent deconjugation and only the molecular ion of the aglycone was detected. For M19, the product ions *m/z* 144 and *m/z* 244 in the MS/MS spectrum suggest a carboxyl function at the defluorinated pentyl chain and further biotransformation at the TMCP ring, which probably is the formation of a hemiacetal structure of a hydroxyl group at the 2′ position and a reactive aldehyde group at the 3′ position. Metabolite M7 (*m/z* 548.2100, RT 6.76min) is likely the M19 glucuronide, because the product ion spectrum of the precursor 548 shows characteristic fragments at *m/z* 144, 218, 244, 354, and 372. The formation of an ether glucuronide, which is more stable than an acyl glucuronide, also prevents the hemiacetal ring structure from reopening.

The 4 metabolites with molecular ion *m/z* 360 are depicted in a bold black line in Fig. 2C (M11, *m/z* 360.1980, RT 8.33 min; M13, *m/z* 360.1970, RT 8.54 min; M22, *m/z* 360.1975, RT 9.33 min; and M27, *m/z* 360.1976, RT 12.47 min). As shown previously, a mass shift of 30 Da represents either a carboxylation or an oxidation and an additional ketone formation. Presence of *m/z* 232 in all product ion spectra excludes the possibility of a modification of the fluoropentyl chain. M27, 2′-carboxy-XLR-11, is the most intense metabolite of all observed metabolites. Among the remaining 3 compounds, M13 is clearly more abundant than M11 and M22, which are only minor metabolites. Searching the raw data for *m/z* 536, the mass of the corresponding glucuronide conjugate, revealed that M13 and M22 are insource fragmented glucuronides. Because relevant signals at *m/z* 536 could be seen, the mass of $[MH]^+$ in Table 2 was adjusted accordingly. It is highly probable that M11, which elutes earlier at 8.33 min, is a glucuronide as well. As mentioned before for the hydroxy glucuronides, inclusion of a second chiral center by conjugation with glucuronic acid leads to diastereomers of former identical isomers. This suggests that M11 and M13 are 2 diastereomers of 2′-carboxy-XLR-11 glucuronide, M13 being the primary isomer. M22, which shows the same fragments as the other 3 metabolites, is probably generated by hemiacetal formation followed by glucuronidation.

Dioxidation followed by internal dehydration is the proposed biotransformation for 2 metabolites (M23, *m/z* 356.1858, RT 9.64 min and M30, *m/z* 344.2019, RT 13.84 min) (both in grey in Fig. 2C). Both metabolites have an additional aliphatic ring and differ only in the pentyl side chain that is either fluorinated or carboxylated.

Understanding synthetic cannabinoid metabolism is necessary for many reasons. Most importantly, identification of metabolites provides the basis for the development of analytical methods, enabling toxicologists and clinicians to correctly link observed adverse effects to the causative designer drug. Combining epidemiological and clinical data from poison control centers, emergency departments, and police reports with synthetic cannabinoid metabolite concentrations will improve our understanding of the drugs' pharmacodynamic effects and pharmacokinetics, and permit us to better interpret analytical results of these new designer drugs. These data also are critically important for future controlled drug administration studies, should they become possible, and for evaluating the contributions of metabolites that may contribute to pharmacodynamic effects. Chimalakonda et al. showed that some synthetic cannabinoid metabolites may have cannabinoid receptor affinities similar to those of the parent drug *(10)*.

Conclusions

In summary we define here for the first time XLR-11 human metabolism by human hepatocyte culture, high-resolution MS, and software-assisted data mining. XLR-11 is one of the most prevalent new synthetic cannabinoids. Identifying intake of this new designer drug requires that the major metabolites expected in urine are defined. These are the first data on XLR-11 metabolites giving clinical and forensic toxicologists a basis for developing analytical methods, identifying XLR-11 exposure, and interpreting urine results. This approach provides a powerful tool for rapid identification of metabolites of unknown synthetic cannabinoids and will be used for metabolite identification of these and other emerging designer drugs.

Author Contributions: *All authors confirmed they have contributed to the intellectual content of this paper and have met the following 3 requirements: (a) significant contributions to the conception and design, acquisition of data, or analysis and interpretation of data; (b) drafting or revising the article for intellectual content; and (c) final approval of the published article.*

Authors' Disclosures or Potential Conflicts of Interest: *Upon manuscript submission, all authors completed the author disclosure form. Disclosures and/or potential conflicts of interest:*

Employment or Leadership: None declared.
Consultant or Advisory Role: None declared.
Stock Ownership: None declared.
Honoraria: None declared.
Research Funding: Materials transfer agreement between National Institutes of Health and AB Sciex and the Intramural Research Program, National Institute on Drug Abuse, and National Institutes of Health.
Expert Testimony: None declared.
Patents: None declared.

Role of Sponsor: The funding organizations played no role in the design of study, choice of enrolled patients, review and interpretation of data, or preparation or approval of manuscript.

References

1. Frost JM, Dart MJ, Tietje KR, Garrison TR, Grayson GK, Daza AV, et al. Indol-3-ylcycloalkyl ketones: effects of N1 substituted indole side chain variations on CB(2) cannabinoid receptor activity. J Med Chem 2009;53:295–315.
2. Huffman JW. Cannabimimetic indoles, pyrroles and indenes. Curr Med Chem 1999;6:705–20.
3. Makriyannis A, Deng H. Cannabimimetic indole derivatives. Patent WO/2001/028557, 2001.
4. Sedefov R, Gallegos A, Kind L, Lopez D, Auwarter V, Hughes B. EMCDDA 2009 thematic paper - understanding the 'Spice' phenomenon. Office for Official Publications of the European Communities, 2009. www.emcdda.europa.eu/attachements.cfm/att_80086_EN_SpiceThematicpaperfinalversion.pdf (Accessed August 2013).
5. Psychonaut Web Mapping Research Group. Spice report. Institute of Psychiatry, King's College London, 2009. www.psychonautproject.eu/documents/reports/Spice.pdf (Accessed August 2013).
6. American Association of Poison Control Centers. Synthetic marijuana data, 2013. http://www.aapcc.org/alerts/synthetic-marijuana/ (Accessed August 2013).
7. Substance Abuse and Mental Health Services Administration, Center for Behavioral Health Statistics and Quality. The DAWN report: drug-related emergency department visits involving synthetic cannabinoids, 2012. www.samhsa.gov/data/2k12/DAWN105/SR105-synthetic-marijuana.pdf (Accessed August 2013).
8. Center for Substance Abuse Research. CESAR fax: synthetic marijuana third most reported substance used by US high school students. 2013. www.cesar.umd.edu/cesar/cesarfax/vol22/22–17.pdf (Accessed August 2013).
9. Stogner JM, Miller BL. A spicy kind of high: a profile of synthetic cannabinoid users. J Subs Use 2013;0:1–7.
10. Chimalakonda KC, Seely KA, Bratton SM, Brents LK, Moran CL, Endres GW, et al. Cytochrome P450-mediated oxidative metabolism of abused synthetic cannabinoids found in K2/Spice: identification of novel cannabinoid receptor ligands. Drug Metab Dispos 2012;40:2174–84.
11. Grigoryev A, Kavanagh P, Melnik A. The detection of the urinary metabolites of 1-[(5-fluoropentyl)-1h-indol-3-yl]-(2-iodophenyl)methanone (AM-694), a high affinity cannabimimetic, by gas chromatography-mass spectrometry. Drug Test Anal 2012;5:110–5.
12. Grigoryev A, Kavanagh P, Melnik A. The detection of the urinary metabolites of 3-[(adamantan-1-yl)carbonyl]-1-pentylindole (AB-001), a novel cannabimimetic, by gas chromatography-mass spectrometry. Drug Test Anal 2012;4:519–24.
13. Grigoryev A, Melnik A, Savchuk S, Simonov A, Rozhanets V. Gas and liquid chromatography-mass spectrometry studies on the metabolism of the synthetic phenylacetylindole cannabimimetic JWH-250, the psychoactive component of smoking mixtures. J Chromatogr B Analyt Technol Biomed Life Sci 2011;879:2519–26.
14. Hutter M, Broecker S, Kneisel S, Auwarter V. Identification of the major urinary metabolites in man of seven synthetic cannabinoids of the aminoalkylindole type present as adulterants in "herbal mixtures" using LC-MS/MS techniques. J Mass Spectrom 2012;47:54–65.
15. Kavanagh P, Grigoryev A, Melnik A, Simonov A. The identification of the urinary metabolites of 3-(4-methoxybenzoyl)-1-pentylindole (RCS-4), a novel cannabimimetic, by gas chromatography-mass spectrometry. J Anal Toxicol 2012;36:303–11.
16. Sobolevsky T, Prasolov I, Rodchenkov G. Detection of urinary metabolites of AM-2201 and UR-144, two novel synthetic cannabinoids. Drug Test Anal [Epub ahead of print 2013 Oct 5]..
17. Department of Justice, Drug Enforcement Administration. Schedules of controlled substances: temporary placement of three synthetic cannabinoids into schedule, Federal Register Vol. 78, 2013. http://www.gpo.gov/fdsys/pkg/FR-2013-05-16/html/2013-11593.htm (Accessed August 2013).
18. Shevyrin V, Melkozerov V, Nevero A, Eltsov O, Morzherin Y, Shafran Y. Identification and analytical properties of new synthetic cannabimimetics bearing 2,2,3,3-tetramethylcyclopropanecarbonyl moiety. Forensic Sci Int 2012;226:62–73.
19. Uchiyama N, Kawamura M, Kikura-Hanajiri R, Goda Y. URB-754: a new class of designer drug and 12 synthetic cannabinoids detected in illegal products. Forensic Sci Int 2012;227:21–32.
20. European Monitoring Centre for Drugs and Drug Abuse. European database on new drugs. https://ednd-cma.emcdda.europa.eu.
21. NMS Labs. Designer drug trends report: changes in the designer drug market Spring 2012. www.nmslabs.com/uploads/PDF/DesignerDrugSpringUpdate_BKLWebinar_May2012.pdf (Accessed August 2013).
22. Center for Disease Control and Prevention (CDC). Acute kidney injury associated with synthetic cannabinoid use. MMWR Morb Mortal Wkly Rep 2013;62:93–8.
23. Thornton SL, Wood C, Friesen MW, Gerona RR. Synthetic cannabinoid use associated with acute kidney injury. Clin Tox 2013;51:189–90.
24. Kavanagh P, Grigoryev A, Savchuk S, Mikhura I, Formanovsky A. UR-144 in products sold via the internet: identification of related compounds and characterization of pyrolysis products. Drug Test Anal 2013;5:63892.
25. Molinspiration Property Calculation Service. www.molinspiration.com